Nanoscale

Accepted Manuscript

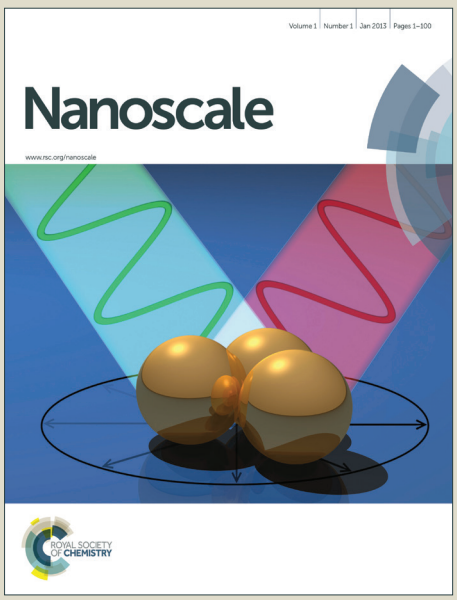

ROYAL SOCIETY OF CHEMISTRY

www.rsc.org/nanoscale

All solution Processed Low Turn-on Voltage Near Infrared LEDs Based on Core-Shell PbS/CdS Quantum Dots with Inverted Device Structure

Rafael S. Sanchez,[1] Enrico Binetti,[2,#] Jose A. Torre,[1] G. Garcia-Belmonte,[1] Marinella Striccoli,[2] Ivan Mora-Sero,[*,1]

[1] *Photovoltaic and Optoelectronic Devices Group, Departament de Física, Universitat Jaume I, 12071 Castelló, Spain.*

[2] *CNR-IPCF Division of Bari, c/o Department of Chemistry, via Orabona 4, 70126 Bari, Italy*

 # Author Present Address: Institute for Composite and Biomedical Materials, National Research Council, Via Sommarive, 14 - 38123 Trento, Italy.

[*]Corresponding Author: sero@uji.es

Abstract

Colloidal Semiconductor Quantum Dots (QDs) are extraordinarily appealing for the development of light emitting devices (LEDs) due to tunable and pure color emission, brightness and solution processability. This last advantage of the QD-LEDs is even more evident in the field of infrared emission where the devices currently used are prepared by high cost epitaxial techniques. Here we show the fabrication of low cost NIR QD-LEDs based on high quantum yield core/shell PbS/CdS QDs and a novel inverted device structure. Devices are produced using SnO_2:F (FTO) as conductive transparent contact, nanostructured TiO_2 as electron transport layer (ETL) and poly(3-hexylthiophene) P3HT as hole transport layer (HTL). Despite the roughness of this ETL, the obtained external quantum efficiencies (EQE) are similar to previously reported values, obtained with regular configuration and more expensive ITO substrates. A turn-on voltage as low as the QD band gap (1.47 eV) is achieved for a large area (1.54 cm^2) and relatively stable QD-LEDs.

TOC:

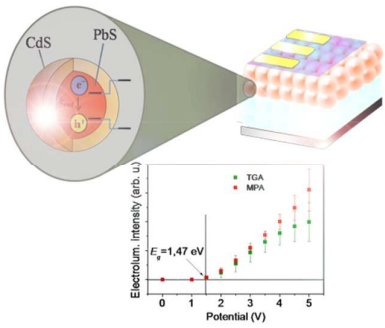

Keywords: Quantum Dots, Core-shell, NIR LED, PbS, inverted configuration

Abstract

Colloidal quantum dots (QDs) present very unique and suitable electro-optical properties, such as wide and tunable absorption and very narrow and intense emission spectra, for the development of optoelectronic devices. [1-3] In addition, they can be dispersed in solvents, thank to the presence of organic ligands on their surface, and easily processed at room temperature conditions using low-cost techniques. Importantly, a wide variety of parameters such as solubility,[4] mechanical resistance of the films,[5] inter-dot distance,[6] photo-luminescence quantum yield (PL QY) [2, 7] or electrical conductivity,[8] among others characteristics, can be controlled by varying the QD surface passivation agents used for the film preparation, which is usually based on the ligand exchange layer-by-layer deposition methodology.

The PL QY of QDs in solution is a crucial parameter to be maximized in order to produce highly efficient electroluminescent devices, since film deposition of QDs typically induces a significant quenching of the luminescent properties through non-radiative recombination pathways, *e.g.* Förster resonant energy transfer (FRET)[9] or Auger recombination,[10, 11] among other feasible mechanisms. In this respect, core-shell QDs present some advantages compared to those composed by a single material. On the one hand, they have enhanced luminescent characteristics, due to the efficient surface passivation of the inorganic shell, reaching in some cases values of PL QYs close to 1.[3, 12] On the other hand, core-shell or core-multishell QDs show outstanding photochemical and thermal stability, which is a crucial requirement for the fabrication of stable and long-living light emitting devices.[2, 7]

Although much effort is being devoted to exploit QDs in LED technology, there are still remaining issues and limitations to be considered and improved: *i)* high turn-on voltages; *ii)* low device efficiency; *iii)* non-negligible parasitic electroluminescence from adjacent layers; *iv)* charge accumulation and subsequent loss of light emission due to an inefficient carrier injection into the QDs;[2] *v)* difficulty of preparing large active area devices due to defects and/or inhomogeneities during the deposition process. Therefore, apart from the optimization of the electro-optical properties of the active layers, the election of the suitable materials, i.e. electron- or hole-transport layers, QDs linkers and metal contacts, and the use of the proper device configuration play a crucial role on the ultimate performance of the devices.

Furthermore, despite the interest of NIR LEDs for communications, sensing, night vision screens or labeling, sensible lower amount of research on this topic has been carried out in comparison with LEDs in the visible range.[3, 6,13] Here we demonstrate the successful fabrication of NIR QD-LEDs using colloidal

NIR emitting core-shell nanocrystals based on metal chalcogenides, which are constituted by a PbS core covered with a shell of CdS, a wider gap material, See Fig. 1b. Among the lead chalcogenides, PbS has a larger band-gap than PbSe and PbTe, therefore this material does not require ultra-small sized nanocrystals to tune the gap to the NIR spectral region.[14] The CdS shell generates higher PL QYs,[15] while enhancing notably the photochemical[16] and thermal stability.[17] The NIR QD-LEDs are processed completely by solution techniques using a novel inverted configuration, exhibit a very low turn-on voltage without parasitic electroluminescence and high active area devices can be produced.

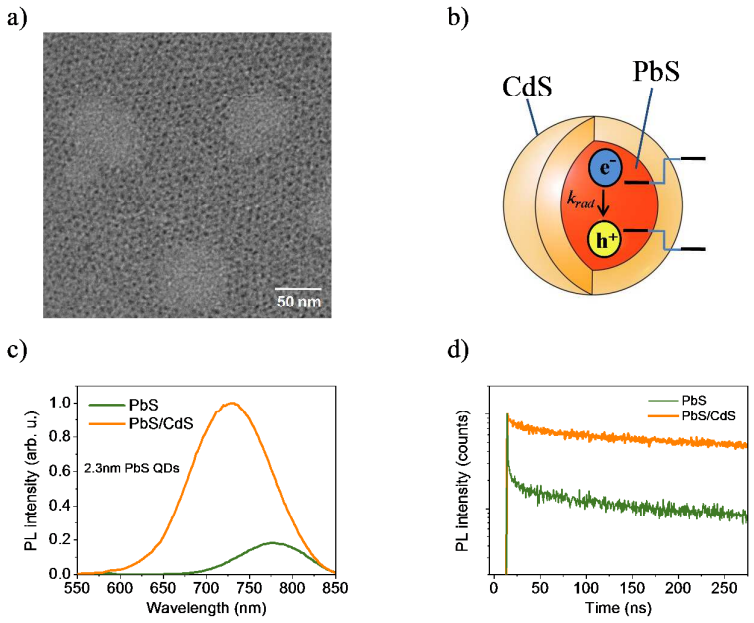

Figure 1.- Characterization of the PbS and PbS/CdS nanocrystals. **(**a) TEM image of PbS/CdS QDs 3.0 nm in diameter. (b) Schematic structure and relative energy levels of the core-shell QD. (c) Emission spectra of PbS and PbS/CdS QDs (2.3 nm in diameter) under excitation light at 500 nm. (d) Time-resolved PL decay of PbS and PbS/CdS QDs (2.3 nm in diameter), excited with a 200 ps laser source at 375 nm.

The core-shell QDs were synthesized by adopting some modifications to reported procedures.[18, 19] The synthetic procedure was divided in two steps. At first, oleic acid capped PbS QDs of 2.3 and 3 nm in diameter were synthesized and purified, and, subsequently, an external shell of CdS was grown on their surface by means of a cation exchange methodology, see supporting information for further experimental details. The QDs were exhaustively characterized and, as it is shown in the TEM image (Fig. 1a), the synthetic methodology produces well dispersed round-shaped QDs with good size uniformity. An

illustrative scheme of the type I core-shell morphology is shown in Fig. 1b. The formation of the CdS shell induces a notable enhancement of the photoluminescent properties of the QDs due to an efficient surface defects passivation, Fig. 1c.[20] Therefore, the PL QY in solution of the Oleate-capped QDs is increased almost a twenty-fold factor after the CdS shell growth (from 1.1% to 20% for PbS and PbS/CdS in hexane, respectively) and the stability of the QDs in terms of photo-oxidation reactions is enormously enhanced. Besides, a significant hypsochromic shift of the PL peak is observed after the shell growth, Fig. 1c, which is usually ascribed to the reduction of the core diameter due to the Pb to Cd cation exchange.[21] Type I core/shell QD configuration provokes the localization of the electrons and holes wavefunctions at the core of the nanocrystals, thus favoring the radiative recombination of the charge carriers.[18] Consequently, the excited state dynamics are strongly influenced by the presence of the CdS shell. Fig. 1d shows the time-resolved PL decays of PbS and PbS/CdS QDs in which the core-shell QDs show a slower decay kinetics (average lifetime of 424 ns for PbS QDs vs. 742 ns for core/shell), due to suppression of non-radiative decay processes arising from an effective passivation of the surface defects, see supplementary information (SI1).[22]

With the aim of preparing NIR QD-LEDs, we propose a nanostructured TiO_2 electrode as an electron-transport material (ETM), due to the suitable energy level alignment with PbS nanocrystals[23] and its high refractive index (n_{TiO2} = 2.7),[24] both properties that contribute to enhance the charge injection and light extraction from the devices, respectively.[21, 25] In fact higher efficiencies have been obtained if TiO_2 mesoporous layer is used instead of just TiO_2 compact layer, probably due to an enhancement of light coupling out efficiency. In addition, TiO_2 films can be easily prepared and show high mechanical, chemical and photochemical stability. The high chemical stability ensures a perfect compatibility with acidic molecules (as Thioglycolic Acid (TGA), 3-Mercaptopropionic Acid (MPA)) to perform the ligand exchange of QDs. The inverted device configuration is exploited, as it allows the use of cost efficient TiO_2 and the deposition of the hole transport material (HTM) on the top of the QD layer, thus avoiding its degradation or desorption during the deposition of the QD film.[2] Note that the use of TiO_2 requires annealing at 450ºC, see supporting information. At such temperature the ITO film changes its optoelectronic properties, which is noticeable in a darkener of the color and a significant decrease of the conductivity, being necessary the use of an alternative transparent conducting oxide as FTO.

A photograph of a working QD-LED and a schematic of the device structure correlated with the cross-sectional scanning electron microscopy (SEM) is shown in Fig. 2a. These devices consist of a patterned FTO cathode, sensibly less expensive than conventional ITO, a 100-nm TiO_2 blocking layer, a 500-nm nanostructured TiO_2 layer as ETM, a 250-nm QD layer as emissive layer, a thin layer of poly(3-hexylthiophene) P3HT as HTM and a 60-nm gold layer as anode, see Fig. 2a. The energy-dispersive X-ray analysis (EDX) of the device is shown in the supporting information (Fig. S2). The structure of our devices was designed to achieve efficient charge injection into the core-shell QDs promoted by applying a very low external potential, since the conduction band (CB) and valence band (VB) of PbS match, in terms of energy level alignment, the utilization of TiO_2 as ETM, P3HT as HTM and gold as back contact.[26] In addition, this configuration allows for an all-solution process with cost effective precursors.

The PL of QD layers and the ultimate performance of the devices have been studied by using different linkers, depending on the length of the alkyl chain and the nature of their functional groups, see Fig. 2c. A series of bi-functional organic linkers has been employed for the QD layer assembly, including TGA, MPA, 1,2-ethanedithiol (EDT) and ethylenediamine (ETDA). EDT and ETDA quenched partially or completely the fluorescence of the QD films, since thiol and amine groups act as hole traps.[27, 28] In contrast, the QD films grown with TGA and MPA as capping agents showed high photoluminescent characteristics. The TGA films and devices were taken as reference for optimizing the different parameters in this study. Fig. 2b shows the absorption and PL spectra of the 3nm PbS/CdS nanocrystals in solution (inset) and deposited on a film using TGA as linker. The optical band-gap (E_g) of the QDs in solution (hexane) was estimated to be 1.47 ± 0.02 eV from the intersection wavelength value between the normalized absorption and emission spectra. It is observed that the Stoke's shift, *i.e.* the energetic difference between the positions of the band maxima of the absorption and emission spectra, is increased from 0.19 eV to approximately 0.32 eV after the film deposition, what could be ascribed to the energy relaxation processes via phonon emission and/or to the generation of defects, probably, arising from the ligand exchange and nanocrystal assembly.[29-31] This observation together with the larger inter-dot interaction after the growth of the QD film is consistent with red-shift of the emission spectra of QDs ($\Delta\lambda_{em} \approx 30$ nm) after the deposition using TGA as linker, which may contribute to lower significantly the light emissive properties of the QDs in the film.

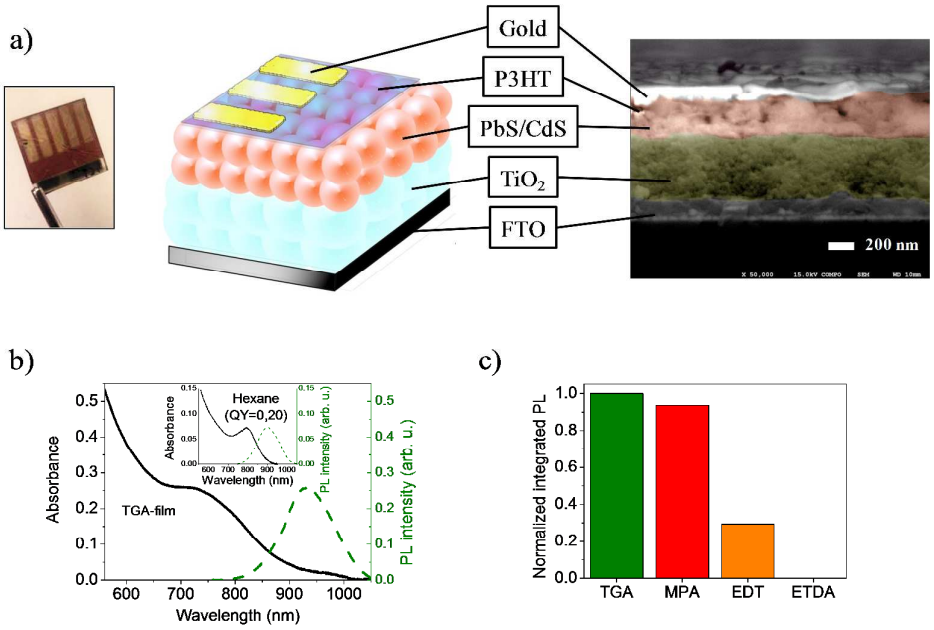

Figure 2.- Structural design of the QD-LEDs. (a) Photograph of a five working contacts QD-LED device and the schematic structural configuration of a device showing the different layers of materials correlated with a cross-section SEM image. (b) Absorption and PL spectra of the PbS/CdS QDs in solution (inset) and as QD film using TGA as linker. The PL QY value was measured in hexane (λ_{exc}= 650 nm) by the comparative method using the dye IR125 as emission reference (PL QY = 4.3% in methanol). (c) Integrated photoluminescence intensity of the PbS/CdS QD (3.0 nm in diameter) films (λ_{exc}= 532 nm) deposited using the corresponding capping agents (TGA, MPA, EDT and ETDA).

Fig. 3a shows the dependence of the radiance spectra of the TGA based device with the increasing potential in the range comprised between 0 and +5 V. The electroluminescence spectra are situated at the same spectral position and present exactly the same shape than PL measurements, see supporting information (Fig. S3), which indicates the absence of parasitic electroluminescence in the ETM or HTM layers. The results indicate that charge carriers are directly injected into the QD layer and undergo subsequent radiative recombination, thus avoiding the exciton generation on the polymer and subsequent energy transfer to the nanocrystals. All the devices prepared using EDT and ETDA for the QD film growth did not show any electroluminescence signal at the studied potential range. This observation is in good agreement with the low PL properties of these films, Fig. 2c. The electroluminescence intensity of the TGA and MPA samples is shown in Fig. 3b, and they exhibit turn-on voltages as low as the QD band-gap, indicating a null potential barrier for electron and hole injection into the PbS/CdS QDs. This result is especially significant taking into account the roughness of the cathode (FTO and mesoporous TiO_2). QD-

LEDs present a good rectifying behavior, see Fig. 3c. Root Mean Square (RMS) roughness of commercial ITO is around 2.5 nm,[32] while RMS of FTO is one order of magnitude higher.[33] The length of the alkyl chain of the ligands has a significant effect on the electrical properties of the QD films.[6] Shorter hydrocarbon chains give rise to higher current densities. However, the external quantum efficiency values (EQE), *i.e.* the ratio between the emitted photons and the electrons flowing through a device, were increased significantly for the longer alkyl chain capping agents, see Fig. 3d.[6] It worth to mention that the EQE's obtained for the MPA based devices are similar to those reported in a previous work using also MPA-ligand PbS QDs and exploiting the direct device configuration on ITO substrates, see Fig. 3d.[6] Devices with surface area as large as 1.54 cm^2 have been prepared with just a 4-fold decrease of the EQE despites the area has been enlarged 7 times, compared to the devices with active area of 0.224 cm^2, Fig. 3d. In addition, the response time and the light out-put angle of the devices have been measured (t= 2.3 ms and Ω= 1.47 rad, respectively), see supporting information (Fig. S4 and S5) for further details.

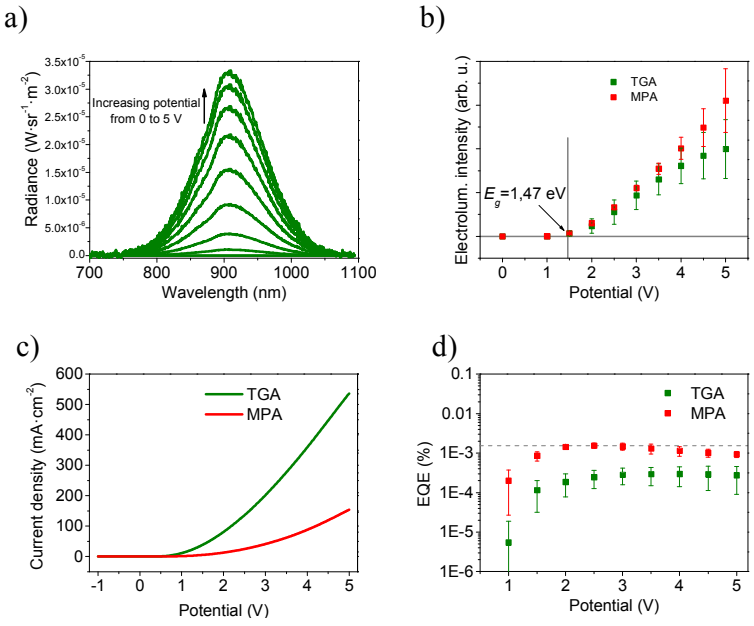

Figure 3.- Opto-electronic characterization of QD-LEDs. (a) Radiance spectra of the TGA based device at different applied potentials (from 0 to +5 V). (b) Electroluminescence intensity of the samples prepared with TGA and MPA as capping agents. The turn-on potentials were calculated from the linear fitting of the electroluminescence intensity values by means of an extrapolation towards the abscissa edge. (c) *J/V* curves of the TGA and MPA devices from -1V to +5V. PbS/CdS QDs (3.0 nm in diameter). (d) External quantum efficiency (EQE) of the TGA and MPA based devices at the different applied bias. The error bars shown in the graphs b and d indicate the standard deviation at each potential arising from the measurement of five different devices for TGA and MPA, respectively. The grey

dashed line indicates the average EQE obtained in a previous work in the literature for PbS QD-LEDs with MPA in conventional configuration.[6] Note, that this information is just included as a reference value as it is not straight forward to compare directly core QDs and core/shell QDs of different size.

Finally, the stability issues of the QD-LEDs have been analyzed. The prepared devices present a surprising good stability, with intermittent use, during months and stored under air conditions. Under continuous work use, the stability is limited due to an electroluminescence drop. The use of HTM did not have any significant impact on the electroluminescent intensity, turn-on voltage or EQE values, but increased dramatically the lifetime of the devices, see supporting information (Fig. S6). Therefore, the P3HT is supposed to favor the charge extraction from the QD layer. At constant applied bias (3V) under air atmosphere conditions and without encapsulation, almost the 50% of the initial electroluminescence was preserved after 10 hours of operation, see Fig 4. It is interesting to see that the decay of electroluminescence correlates with the decay observed in current, pointing out to a decrease of the emission due to a current decrease instead of QD degradation, as stability under intermittent use corroborates. This fact suggests that further optimization of the QD-LED can be achieved by using different HTL and/or deposition processes, which is clearly compatible with the inverse configuration of our devices. The current decrease over the time is probably due to charge trapping at bulk QD film and it is under current study.

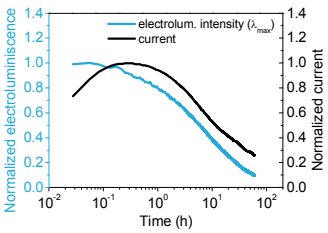

Figure 4.- Operational lifetime. Electroluminescence intensity at the λ_{max} and electric current monitoring of the device during 60 hours under continuous operation. Measurement carried out at continuous applied bias of 3V under air atmosphere conditions and without encapsulation.

In summary, all solution processed NIR QD-LEDs with inverse configuration based on highly luminescent core/shell PbS/CdS QDs have been produced. The PbS/CdS QDs are characterized by tunable and intense PL, high photostability and solution processability. Low cost FTO and TiO_2 layer has

been used as ETL, instead of the conventional ITO. Despites the roughness of ETL, the measured EQE with MPA linker is similar to the previously reported values with direct configuration and ITO substrate. In addition, our methodology allows the preparation of large active area devices with a turn-on potential as low as QD band gap, and present excellent lifetime (months) under intermittent use and a relatively limited performance under continuous use (50% electroluminescence drop after 10 hours). We do believe that the efficiency obtained with this new configuration can be even enhanced specially by using alternative HTL. The use of a wide variety of HTL and deposition methods is reachable by exploiting the inverse configuration.

ACKNOWLEDGMENTS

This work was partially supported by Generalitat Valenciana (ISIC/2012/008), and FP7 European project ORION (Large CP-IP 229036-2), and Universitat Jaume I project 12I361.01/1. We thank SCIC from Universitat Jaume I for the help with SEM measurements, and R. Comparelli from CNR IPCF for TEM measurements.

References:

1. K.-S. Cho, E. K. Lee, W.-J. Joo, E. Jang, T.-H. Kim, S. J. Lee, S.-J. Kwon, J. Y. Han, B.-K. Kim, B. L. Choi and J. M. Kim, *Nat Photon*, 2009, **3**, 341-345.
2. J. Kwak, W. K. Bae, D. Lee, I. Park, J. Lim, M. Park, H. Cho, H. Woo, D. Y. Yoon, K. Char, S. Lee and C. Lee, *Nano Letters*, 2012, **12**, 2362-2366.
3. Y. Shirasaki, G. J. Supran, M. G. Bawendi and V. Bulovic, *Nat Photon*, 2013, **7**, 13-23.
4. F. Dubois, B. Mahler, B. Dubertret, E. Doris and C. Mioskowski, *Journal of the American Chemical Society*, 2006, **129**, 482-483.
5. L. Zhou, C. Gao and W. Xu, *Journal of Materials Chemistry*, 2010, **20**, 5675-5681.
6. L. Sun, J. J. Choi, D. Stachnik, A. C. Bartnik, B.-R. Hyun, G. G. Malliaras, T. Hanrath and F. W. Wise, *Nat Nano*, 2012, **7**, 369-373.
7. X. Wang, W. Li and K. Sun, *Journal of Materials Chemistry*, 2011, **21**, 8558-8565.
8. G. D. Lilly, A. C. Whalley, S. Grunder, C. Valente, M. T. Frederick, J. F. Stoddart and E. A. Weiss, *Journal of Materials Chemistry*, 2011, **21**, 11492-11497.
9. T.-W. F. Chang, A. Maria, P. W. Cyr, V. Sukhovatkin, L. Levina and E. H. Sargent, *Synthetic Metals*, 2005, **148**, 257-261.
10. W. K. Bae, Y.-S. Park, J. Lim, D. Lee, L. A. Padilha, H. McDaniel, I. Robel, C. Lee, J. M. Pietryga and V. I. Klimov, *Nat Commun*, 2013, **4**.
11. D. Bozyigit, O. Yarema and V. Wood, *Advanced Functional Materials*, 2013, **23**, 3024-3029.
12. J. M. Pietryga, D. J. Werder, D. J. Williams, J. L. Casson, R. D. Schaller, V. I. Klimov and J. A. Hollingsworth, *Journal of the American Chemical Society*, 2008, **130**, 4879-4885.
13. M. Stevenson, J. Kamplain, J. Perkins, Z. Zhou, M. Bunda, S. Coe-Sullivan, J. S. Steckel and P. Kazlas, IR quantum dots for defense applications, 2013.
14. L. Bakueva, S. Musikhin, M. A. Hines, T.-W. F. Chang, M. Tzolov, G. D. Scholes and E. H. Sargent, *Applied Physics Letters*, 2003, **82**, 2895-2897.

15. O. Chen, J. Zhao, V. P. Chauhan, J. Cui, C. Wong, D. K. Harris, H. Wei, H.-S. Han, D. Fukumura, R. K. Jain and M. G. Bawendi, *Nat Mater*, 2013, **12**, 445-451.
16. H.-J. Zhan, P.-J. Zhou, R. Ma, X.-J. Liu, Y.-N. He and C.-Y. Zhou, *J Fluoresc*, 2013, 1-9.
17. W. Guo, J. J. Li, Y. A. Wang and X. Peng, *Journal of the American Chemical Society*, 2003, **125**, 3901-3909.
18. M. V. Kovalenko, R. D. Schaller, D. Jarzab, M. A. Loi and D. V. Talapin, *Journal of the American Chemical Society*, 2012, **134**, 2457-2460.
19. M. S. Neo, N. Venkatram, G. S. Li, W. S. Chin and W. Ji, *J. Chem. Phys. C*, 2010, **114**, 18037-18044.
20. M. S. de la Fuente, R. S. Sánchez, V. González-Pedro, P. P. Boix, S. G. Mhaisalkar, M. E. Rincón, J. Bisquert and I. Mora-Seró, *J. Chem. Phys. Lett.*, 2013, **4**, 1519-1525.
21. P. Reiss, M. Protière and L. Li, *Small*, 2009, **5**, 154-168.
22. M. J. Fernée, A. Watt, J. Warner, S. Cooper, N. Heckenberg and H. Rubinsztein-Dunlop, *Nanotechnology*, 2003, **14**, 991.
23. B.-R. Hyun, Y.-W. Zhong, A. C. Bartnik, L. Sun, H. D. Abruña, F. W. Wise, J. D. Goodreau, J. R. Matthews, T. M. Leslie and N. F. Borrelli, *ACSNano*, 2008, **2**, 2206-2212.
24. F. W. Mont, J. K. Kim, M. F. Schubert, E. F. Schubert and R. W. Siegel, *Journal of Applied Physics*, 2008, **103**, -.
25. T. Tsutsui, M. Yahiro, H. Yokogawa, K. Kawano and M. Yokoyama, *Advanced Materials*, 2001, **13**, 1149-1152.
26. S. H. Im, H.-J. Kim, S. W. Kim, S.-W. Kimb and S. I. Seok, *Energy Environ. Sci.*, 2011, **4**, 4181–4186.
27. A. A. Cordones and S. R. Leone, *Chemical Society Reviews*, 2013, **42**, 3209-3221.
28. S. Jeong, M. Achermann, J. Nanda, S. Ivanov, V. I. Klimov and J. A. Hollingsworth, *Journal of the American Chemical Society*, 2005, **127**, 10126-10127.
29. N. O. Dantas, P. M. N. de Paula, R. S. Silva, V. López-Richard and G. E. Marques, *Journal of Applied Physics*, 2011, **109**, -.
30. M. J. Fernée, E. Thomsen, P. Jensen and H. Rubinsztein-Dunlop, *Nanotechnology*, 2006, **17**, 956.
31. J. H. Warner, E. Thomsen, A. R. Watt, N. R. Heckenberg and H. Rubinsztein-Dunlop, *Nanotechnology*, 2005, **16**, 175.
32. Y. Yang, Q. Huang, A. W. Metz, J. Ni, S. Jin, T. J. Marks, M. E. Madsen, A. DiVenere and S. T. Ho, *Advanced Materials*, 2004, **16**, 321-324.
33. T.-H. Fang and W.-J. Chang, *Applied Surface Science*, 2003, **220**, 175-180.